Original scientific paper

QUASI-STATIC INDENTATION BEHAVIOR
OF GFRP WITH MILLED GLASS FIBER FILLER
MONITORED BY ACOUSTIC EMISSION

Kannivel Saravanakumar[1], Balakrishnan Sai Lakshminarayanan[1], Vellayaraj Arumugam[1], Carlo Santulli[2], Ana Pavlovic[3], Cristiano Fragassa[3]

[1]Department of Aerospace Engineering, MIT campus, Chromepet, Anna University, India
[2]School of Architecture and Design, Università of Camerino, Ascoli Piceno, Italy
[3]Department of Industrial Engineering, University of Bologna, Bologna, Italy

Abstract. *This paper aims at investigating the influence of the addition of milled glass fibers upon quasi-static indentation (QSI) properties of glass/epoxy composite laminates. The QSI behavior was experimentally studied by evaluating indentation force, residual dent depth, energy absorbed and size of the damaged area for different indentation depths. Following the QSI tests, the filler-loaded glass/epoxy samples were subjected to three-point bending tests in order to measure residual flexural strength, and the results were compared with the baseline glass/epoxy samples. Both tests were performed with online acoustic emission monitoring in order to observe damage progression and characterize different fracture mechanisms associated with loading. The results show that the filler-loaded laminates exhibit a substantial improvement in the peak force and contact stiffness, with a reduced permanent damage both in terms of depth and of area, in comparison with the baseline ones. It is found that the filler presence offers greater stiffness and higher energy dissipation through toughening mechanisms such as filler debonding/pullout and filler bridging/interlocking.*

Key Words: *Glass/Epoxy, Delamination, Quasi-Static Indentation (QSI), Residual Flexural Strength, Acoustic Emission*

1. INTRODUCTION

Fiber-reinforced composites, made of glass, carbon or even natural fibers, have found their application in several industries such as aerospace, automobile, marine, wind turbines production, etc., due to their high specific stiffness/strength, chemical resistance and fatigue properties, which makes them a suitable alternative for metals [1-3]. On the other side, the composites are susceptible to delamination due to poor mechanical properties through their thickness [4]. This effect is evident, in particular, when adhesion between the fibers and the matrixes is not initially perfect or has deteriorated with use [5]. Especially in the case of low velocity impacts [6] due to external objects, tool drop during service/maintenance, runway debris and other accidental events, etc., localized damage can result in drastic reduction in strength/stiffness and is likely to expand during service. It is noticed that the damage induced in low-velocity impact can be effectively simulated in quasi-static indentation tests regarding their advantage in providing longer times, hence enabling damage evolution monitoring [7, 8]. In practice, the quasi-static indentation tests supply information about contact behavior between the sample and the indenter as well as on the occurrence of sequential damage with varying indenter displacement/depth. Abdallah and Bouver [9] experimentally investigated the damage behavior and effects of permanent indentation on highly oriented composites plates. They observed that the peak force experienced during low velocity impact was higher than in the case of the quasi-static test. However, damage morphology and absorbed energy were equivalent for both tests.

Various works [10, 11] have established correlations between quasi-static indentation and dynamic falling weight impact tests. The damage initiation and propagation were investigated comprehensively by controlling peak force and deformation. The parameters, such as peak load or ultimate load, incident energy, absorbed energy, elastic energy and residual depth, were determined in order to quantify the local damage in the composite materials during quasi-static indentation tests [12, 13]. Arabzadeh and Zeinoiddini [14] studied quasi-static indentation response of flexibly supported pressurized pipes, suggesting a closed-form relationship between indentation force and dent depth by considering different boundary conditions, such as internal pressure soil stiffness and embedment between soil and pipe into their modeling. They observed that the influence of the surrounding soil was prominent when the fluid pressure inside the pipe is very low. Sutherland and Guedes Soares [15] investigated the quasi-static indentation behavior of E-glass/polyester marine laminates observing that the chopped strand mat laminates exhibited better contact stiffness than the woven roving ones. They also report that the large global deflection in thinner samples leads to a larger contact area due to the wrapping of laminate around the indenter. In quasi-static punch shear tests on quasi-isotropic carbon/epoxy, a good correlation between load-displacement response and finite element modeling was reported, indicating that a slope change or a load drop indicates delamination initiation, which propagates through subsequent oscillations: further damage was produced by plug formation exit from the plate [16].

The progressive penetration mechanism of ultra-high molecular weight polyethylene reinforced cross-ply composite laminates was investigated by O'Masta et al. [17]. They observed that sample penetration occurred by tensile ply rupture under the projectile, and higher penetration resistance and onset velocity occurred as the consequence of the sample being end-supported rather than back-supported. The effect of hybridization on

impact and post-impact performance of the composite laminates was investigated by Suresh Kumar et al. [18]. The low-velocity impact behavior was simulated by quasi-static indentation (QSI) tests on quasi-isotropic glass/epoxy, glass/basalt/epoxy (G/B/G, B/G/B) and glass/carbon/epoxy (G/C/G, C/G/C) laminates with acoustic emission monitoring. Addition of basalt fiber and carbon fiber to glass fiber improved indentation damage resistance, while AE monitoring was reported to be a sensitive method to characterize damage evolution in the laminates.

The conventional composite laminates fabricated with thermoset matrix, such as epoxy, suffer from low impact damage resistance, poor fiber/matrix interface bond strength, low fracture toughness, and poor transverse mechanical properties. Their delamination resistance can be enhanced by incorporating micro/nano-sized fillers into the matrix. Toughening mechanisms, such as cavitation, crack pinning, crack deflection, and crack bridging were observed to have improved interlaminar fracture toughness of the composites [19-21].

Acoustic emission monitoring can be effectively used for monitoring/tracking the damage evolution and for identifying/characterizing failure modes in the fiber-reinforced composites laminates during loading [22-24]. Each acquired AE signal bears some relation with the damage mechanisms, in that it is associated with the specific amount of strain energy released during failure. It has been reported that the failure modes can be identified based on the signal-based approach utilizing AE waveforms, fast Fourier transform (FFT) and short time fast Fourier transform (STFFT), while the parametric-based approach uses AE parameters, such as counts, energy, rise time, RMS, signal strength and duration, etc., [25, 26]. Bussiba et al. [27] employed STFFT analysis to discriminate different failure modes and studied sequential damage evolution in composite laminates. Ramirez-Jimenez et al. [28] discriminated damage mechanisms, such as matrix crack, debonding, delamination, and fiber breakage based on the peak frequency analysis. Arumugam et al. [29] investigated the classification of failure modes for different ply orientation sequences, based on the frequency content of AE signals.

This work focuses on investigating the effect of introducing a limited amount of milled glass fiber fillers upon the quasi static indentation behavior and residual performance of glass/epoxy laminates. The damage initiation, progression, and failure mechanism associated with quasi-static indentation and three-point bending test were also discussed with online AE monitoring. The glass/epoxy samples were subjected to quasi-static indentation test at different indentation depths (1 to 6 mm). The indentation test parameters in terms of peak force and absorbed energy, as well as residual (permanent) dent depth and damage area were evaluated, and the results were correlated with those from the baseline samples. The residual strength of the samples was also estimated in order to determine damage tolerance of the composite laminates.

2. EXPERIMENTAL PROCEDURE

2.1. Materials and fabrication of composite laminates

The glass/epoxy composite laminates were fabricated by hand lay-up technique with a cross-ply stacking sequence of $[0°/90°]_{4s}$ configuration. Unidirectional 220 g/m² glass fabric and LY556 epoxy resin with HY951 hardener were used as raw materials and taken in the ratio of 1:1 by weight for fabricating the laminates. Milled glass fibers were

added to the epoxy resin (in a ratio of 5:100 by weight) through sonication and mechanical stirring to distribute them uniformly in the resin. The mixture was then degassed in order to remove entrapped air bubbles. The hardener was added to the mixture at a ratio of 1:10 by weight and further stirred to initiate the curing process. The mixture was then evenly distributed on the glass fabric with the aid of brush and roller to improve fiber impregnation. Correspondingly, baseline glass/epoxy laminates without milled glass fibers were fabricated as above. The laminates, with dimensions of 500 x 500 mm, and nominal thickness of 4.5 (±0.25) mm, were allowed to cure at room temperature for 24 hours; then the samples were cut from them using abrasive water-jet cutting machine. Also filler-loaded samples had the same objective thickness of 4.5 mm, and their weight was in excess with respect to the baseline ones by no more than around 2%, therefore basically included in the experimental error.

2.2. Quasi-Static Indentation test

Quasi-static indentation tests were performed on the Tinius Olsen 100kN Universal Testing Machine at crosshead speed of 1 mm/min. The test was carried out with the indentation fixture as per ASTM D6264/D6264M-17 standard [30], hence with a hemispherical indenter. The glass/epoxy samples with dimensions of 150 x 100 mm rested on the fixture and were clamped at both sides, as shown in Fig. 1. Later, the indentation test was performed directly on the center of the samples. The specimen was indented with a 12.7 mm diameter hemispherical end steel tup. Load-displacement data were recorded *via* the digital data acquisition system from the universal testing machine. Four specimens were tested in all the cases, and the average results were considered. QSI tests were carried out at a predetermined indentation depth of 1, 2, 3, 4, 5 and 6 mm, respectively. Quasi-static indentation behavior and test parameters, such as indentation force, residual dent depth, energy absorbed, contact stiffness and damaged area at different indentation depths were evaluated. The evolution of damage and damage mechanism associated with indentation were monitored with online AE monitoring.
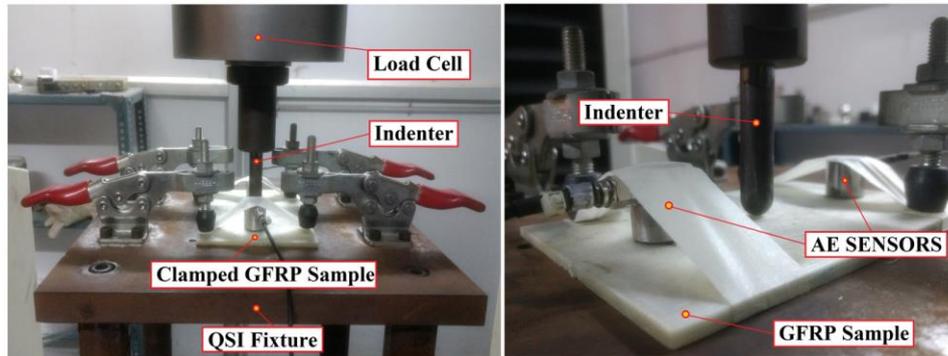
Fig. 1 Quasi-Static Indentation test fixture

2.3. Three-point bending test

Post-indentation flexural tests were performed on glass/epoxy samples, trimmed to a dimension of 150x50 mm using a diamond saw, with three-point bending fixture under displacement control regime. Care was taken to ensure not to damage the indented zone during cutting, according to previous indications supplied by [31-33]. The tests were carried out at a constant cross-head speed of 1 mm/min. The span length was kept equal to 100 mm, and four repetitions were performed for each category of samples. The residual flexural strength was determined from the test, and the results were correlated with the non-indented baseline and filler-loaded samples.

2.4. Acoustic emission monitoring of QSI and FAI

Acoustic emission monitoring was employed during quasi-static indentation tests and flexural after indentation tests. An eight-channel AE system supplied by the Physical Acoustic Corporation (PAC) (Princeton, NJ, USA) with a sampling rate of 3MHz and a 40 dB pre-amplification was used. A threshold of 45 dB was fixed for filtering the ambient noise. Two wideband (WD) sensors in a linear arrangement were employed for AE measurements, and these sensors were attached at a nominal distance of 100 mm along the sample length. High vacuum silicon grease was used as a coupling agent between the sensors and the sample surface. The wave velocity measurements and subsequent calibration of the sensors were performed by the typical pencil lead break test. The average wave velocity for both baseline and filler-loaded glass/epoxy samples were found to be 3120 m/s. The peak definition time (PDT), hit definition time (HDT) and hit lockout time (HLT) were set to be 30 μs, 150 μs, and 300 μs, respectively.

3. RESULTS AND DISCUSSION

3.1. Quasi-static indentation test

Quasi-static indentation tests facilitate investigating the contact behavior between the glass/epoxy laminates and the indenter during loading, as well as monitoring the occurrence of damage sequentially by varying indenter displacement/depth. Usually, the onset of the damage during transverse loading of the composite laminates occurs by: (i) matrix cracking at the local indenter contact point; (ii) debonding between the fiber/matrix interfaces due to transverse matrix cracks; (iii) fiber buckling at the contact point on the compression side; (iv) delamination; and (v) fiber breakage on the tensile side, due to penetration/perforation [15]. The resulting dent force, energy absorbed (Ea), residual dent and size of the damaged area were determined in terms of indentation depth. Moreover, the residual strength of the laminates subjected to quasi-static indentation was evaluated to ensure integrity and damage tolerance of the laminates.
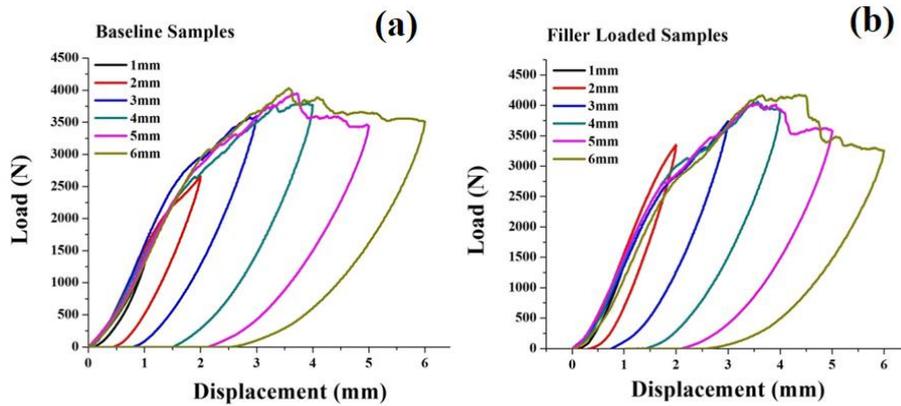
Fig. 2 Load-Displacement curve for different indentation depth: (a) Baseline samples (b) Filler-loaded samples

Figure 2 shows a typical load-displacement curve for the quasi-static indentation test on both baseline and filler-loaded glass/epoxy samples, tested at different indentation depths. The curve profile was initially quasi-linear, which suggested a prevalently elastic behavior: this was followed by the onset of some permanent plastic deformation with increasing indentation displacement. The resistance offered by the samples was observed to increase with indentation depth. Thus, the peak force increases consistently with indentation depth accompanied by a sequence of load drops associated with the occurrence of a significant damage, such as delamination and fiber failure. At a higher indentation depth, the onset of the process leading from fiber disruption to perforation through the appearance of back damage reduces the resistance of the samples through load drops to be ascribed to the indenter producing shear failure and local crushing of fibers during local bending [34]. These load drops are followed by the appearance of a plateau region in the curve, which can be attributed to frictional sliding between the indenter and the sample. In particular, it can be observed that beyond 4 mm no longer any major increase in the peak load is revealed: this was associated with the predominant fiber damage, leading to the appearance of back face damage. Also, the results show that irrespective of indentation depth, the filler-loaded samples exhibited higher load carrying capacity (peak force) than the baseline samples.

The slope of the load-displacement curve during quasi-elastic phase, preceding the first load drop, defines the initial contact stiffness of the glass/epoxy. Further, as the indentation depth increases, non-linear behavior was observed associated with damage accumulation and progression through matrix cracking, while the onset of delamination at a higher delamination depth corresponds to stiffness degradation. More specifically, it was found that the filler-loaded samples exhibit initial contact stiffness of 2181 ± 75 N/mm and delaminated contact stiffness of 955 ± 72 N/mm, against 1902 ± 58 N/mm and 832 ± 75 N/mm for the baseline samples, respectively. In other words, it was observed that the filler-loaded samples exhibited approximately 15% improvement in initial and delaminated contact stiffness, compared to the baseline samples.
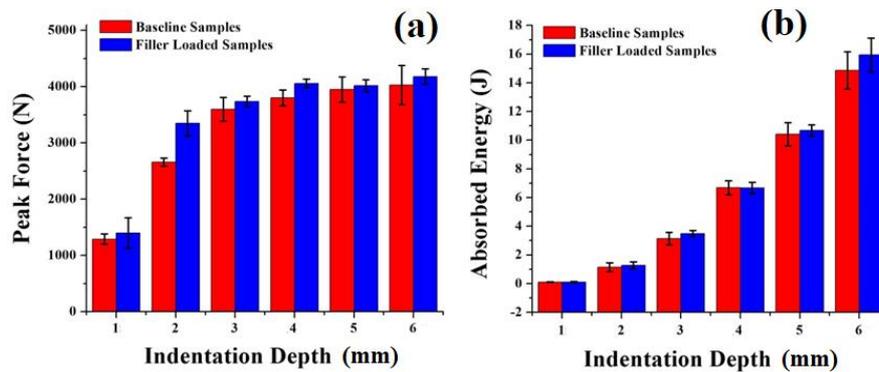
Fig. 3 Comparison of: (a) Peak force (b) Absorbed energy between baseline and filler-loaded samples for different indentation depths

Figures 3 (a) and (b) indicate peak force and absorbed energy variation with respect to indentation depth: both peak force and absorbed energy are slightly higher for the filler-loaded samples; though given the standard deviation, differences are minimal. It can also be observed that while the former shows an abrupt increase at a given indentation depth, particularly between 1 and 2 mm, the latter grows quasi-linearly with it. In general terms, this behavior depends on the fact that the peak force suddenly increases after the contact area overcomes the limit that is related to the dimension of the indenting tup, an evidence which is basically related to its hemispherical geometry [35].

However, at a higher indentation depth, beyond 4 mm, some failure of load-bearing fibers due to induced tensile stress resulted in some reduction in the peak load, which means that the peak loads for both the filler-loaded and the baseline samples were similar. In other words, the influence of the filler on absorbed energy was prominent at a lower indentation depth, while as the indentation depth increases, the contribution of the filler to energy dissipation deteriorates. This was attributed to the damage gradually extending from the matrix to the reinforcement through the intermediate occurrence of some debonding.

What was expected was that the filler-loaded samples would exhibit a reduced damaged area and a smaller residual dent at respective indentation depths in comparison with the baseline ones. The relationship between the peak force and the absorbed energy with a residual (permanent) dent, i.e. the plastic deformation of the samples remaining after unloading for both the baseline and the filler-loaded samples is reported in Fig. 4. In general, both the absorbed energy and the residual dent are increasing with the indentation force. The relation between the peak force and the residual dent indicates that the accumulation of damage is dependent on indentation displacement. The change in the slope was observed to be small/gradual at a lower indentation depth below 3 mm corresponding to matrix cracking and some delamination damage. As the indentation depth increases, the slope of the curve changes rapidly while the peak force remains almost unchanged. The occurrence of fiber breakage with matrix cracking and delamination contributes to an increase in the residual dent depth and with no raise in the peak force, suggesting at this point the transition of failure mechanism from gradual to severe, substantially indicating the occurrence of fiber failure, basically signifying that no resistance is offered by the broken fibers. It is observed that the filler-loaded samples exhibit a lower permanent depth

by an average of 25% than the baseline samples. The filler presence offers improved stiffness and also higher energy dissipation through plastic deformation.

Figure 4 (b) shows the relationship between the permanent dent depth and the absorbed energy for the baseline and the filler-loaded samples. It is well known that the energy absorbed by the samples is utilized for investigating damage development. Thus, the responses of the absorbed energy and the residual dent are dependent and the results show that the trend of the absorbed energy and the residual dent was almost linear till an indentation depth below 4 mm. However, as the indentation depth increases further, the damage is close to saturation in the laminate, which causes marked non-linear behavior. Irrespective of indentation depth, the residual dent depth induced on the filler-loaded samples was consistent and depended upon the absorbed energy, which, in its turn, was higher with the reduced residual dent comparing to the baseline samples. It was observed that the fillers presence enhanced the energy dissipation capacity of the laminates, which was attributed to the toughening mechanism, such as filler debonding/pullout, filler interlocking/ bridging of cracks, as will be seen in Fig. 12.

More indications were expected to come from the measurement of the extent of the damaged, hence delaminated, areas, by non-destructive backlight imaging of the damaged samples with ImageJ software for post-processing: these are reported in Fig. 5 for various indentation depths. The delaminated area had irregular shape and perimeter, despite being centered on the point of indentation. The damage area at the back surface was observed to be greater comparing to the front surface, suggesting a larger disruption if the fiber layers with indenter progress in the laminate, significant for the reduction of flexural performance [36]. The damage area was found to be reduced in the filler-loaded samples for an average of 25% less than for the baseline samples. This is due to the higher rigidity/stiffness offered by the filler-loaded samples resulting in energy dissipation through toughening mechanism such as filler debonding/pullout, filler bridging/interlocking, as will be seen in SEM images. This proves that the filler inclusion resulted in higher energy absorption with a reduced damage area, contributing to enhanced crashworthiness properties of the laminates.

In particular, the effect of the filler introduction on the residual flexural strength after indentation allowed observing that the filler-loaded samples exhibited an average of 18% higher load carrying capacity than the baseline samples (Fig. 6). In particular, three-point bending strength of non-indented laminates was 249 ± 6.5 MPa for baseline ones and 284.5 ± 8.3 MPa for filler-loaded ones. Bending effects are the cause of shear forces leading to delamination propagation toward a free edge during the three-point bending test. This propagation expands from the former delamination damage developed during quasi-static indentation, followed by a newly generated damage. The damage evolution was observed to be gradual on the samples subjected to a low indentation depth showing matrix cracking, and debonding damage followed up by the ultimate failure by fiber breakage at compression or tension side of the samples. The residual flexural strength was observed to reduce gradually by an average of 15% for an indentation depth above 3 mm. In addition, the samples subjected to higher indentation exhibit penetration/ perforation damage leading to a large delamination area and intensive fiber breakage.
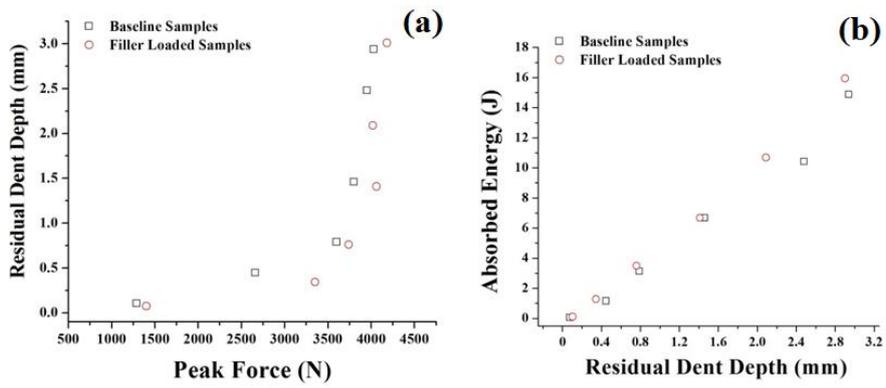
Fig. 4 (a) Peak force vs. Residual dent (b) Absorbed energy vs. Residual dent: comparison between baseline and filler-loaded samples for different indentation depths
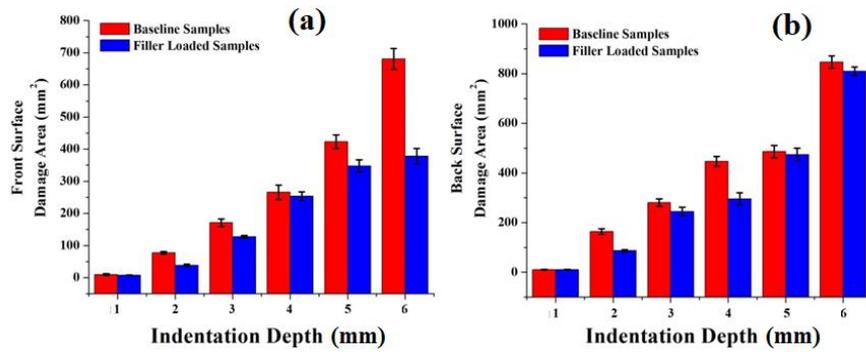
Fig. 5 Damage area at different indentation depth for baseline and filler-loaded samples: (a) Front surface (b) Back Surface
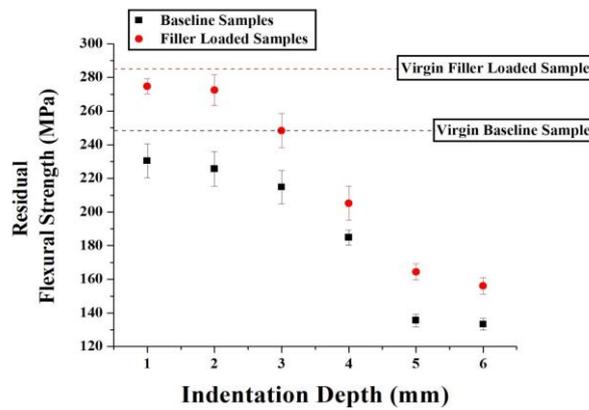
Fig. 6 Residual flexural strength for baseline and filler-loaded samples at different indentation depths

3.2. Acoustic emission monitoring of quasi-static indentation test

Acoustic Emission monitoring is widely employed for inspecting and identifying the sequence and the respective extent of damage mechanisms generated in fiber reinforced composites [37-39]. The microscopic failure events are detected during the tests by AE sensors as AE signals and the frequency analysis is employed to discriminate the failure modes in composite materials. Each AE signal acquired during the tests belongs, therefore, to specific damage modes with a certain amount of strain energy released. The damage mechanisms such as matrix crack, debonding, delamination and fiber breakage were discriminated, based on the peak frequency – cumulative counts vs. time plot. The frequency analysis was performed on the glass/epoxy laminates subjected to quasi-static indentation and flexural after indentation tests.

The load-displacement behavior of the glass/epoxy samples subjected to quasi-static indentation test with acoustic emission monitoring will be discussed in detail, as follows. In general, the AE events initiate after the occurrence of local plastic deformation in the samples. Figures 7 and 8 show Peak frequency & Cumulative Counts vs. time plot of corresponding load-displacement behavior for each indentation depth. The curve profile of the AE cumulative counts – time plot signifies the evolution of damage initiation and progression during loading, as previously discussed, e.g. in [24]. It was observed that the profile of the AE cumulative counts curve changes significantly with subsequent damage as loading progresses. Initially, the damage starts with lower count rates, so that the AE cumulative counts curve is almost flat while the AE signals can be mostly attributed to matrix cracking. Further loading intensifies the progression of matrix cracking within the ply at faster rates, promoting fiber/matrix debonding and fiber breakage, as will be shown in Figs. 10 and 11. Damage accumulation was indicated by a sudden and abrupt increase in the cumulative counts with a change in the slope associated with a major failure such as delamination. Finally, a sharp increase in the cumulative counts with a steep slope corresponds to unstable crack growth, resulting in the ultimate failure of the laminates. Also, the AE signals associated with different failure mechanisms were identified sequentially during the damage evolution from the peak frequency vs. time plots. It is suggested from previous literature that the peak frequency ranges in the GFRP correspond to different damage mechanisms: with some accuracy, these can be defined as 70-120 kHz for matrix cracking, 120-190 kHz for delamination, 190-260 kHz for debonding and 260-320 kHz for fiber failure.

In particular, Figs. 7 (a) and (b) show the results for a lower indentation depth of 1 mm. Both in the baseline and the filler-loaded laminates, the damage initiates in the form of matrix cracking, while fiber/matrix debonding was observed only in the case of the filler-loaded samples; delamination was not yet evident at this indentation depth. This can suggest that the filler-loaded laminates may provide higher energy dissipation through an additional toughening mechanism such as filler/matrix debonding offered by the presence of milled glass fibers. In practical terms, at 1 mm indentation depth, no significant damage was visible in both the baseline and the filler-loaded samples, except minor local indentation at the contact of the indenter. This will be confirmed in Fig. 9, with no delamination/debonding visible for 1 mm indentation depth in the baseline samples.

Figures 7(c) and (d) show the results for an indentation depth of 2 mm, where the damage onset load (or) delamination threshold load was indicated from the incipient point during quasi-static indentation. Typically, the incipient point defines the initial change in the slope or a drop in the load where delamination occurs during testing. The baseline samples

show a change in the slope during 2050N and 1.3mm indentation depth, while the filler-loaded samples indicate a change in the slope only during 2550N and 1.6mm indentation depth. Correspondingly to this load/indentation, damage accumulation was observed attributed to a sudden and abrupt increase in the AE cumulative counts with a change in the slope associated with a major failure, such as debonding/delamination, as observable from the peak frequency-time plot. These failure modes were nominal at 2 mm indentation depth and consequently exhibit a smaller damage area, as seen in Fig. 9. The size of the damaged area, the intensity of damage and relevant damage mechanism were observed to increase with indentation depth.
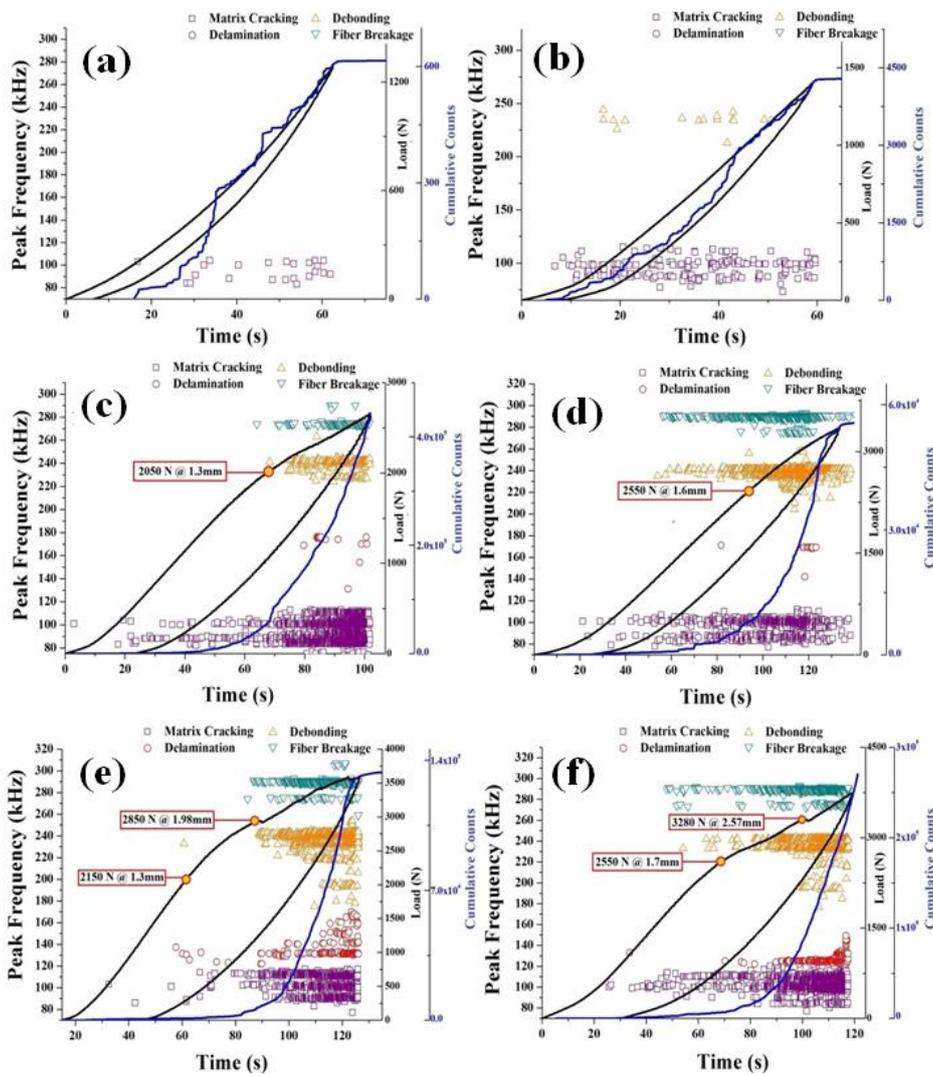
Fig. 7 Peak frequency & Cumulative Counts vs. Time plot of corresponding load-displacement behavior for indentation depth. Baseline samples: (a) 1mm (c) 2mm (e) 3mm & Filler-loaded samples: (b) 1mm (d) 2mm (f) 3mm

The indentation response of the glass/epoxy samples subjected to 3 mm indentation depth can be seen in Figs. 7(e) and (f). In this case, the change of the slope of the load-displacement curve indicates reduced contact stiffness of the material due to the initiation of damage mechanisms, such as matrix cracking, debonding and delamination, as can be seen in Figs. 10 and 11. As previously discussed, the flat region of the curve of the AE cumulative counts indicates the damage initiation stage attributed to low-frequency failure mode matrix cracking, whereas the initiation of delamination in the baseline samples occurred at 2150N and 1.3mm, followed by a sudden load drop at 2850N and 1.98mm, corresponding to the fiber failure, as seen in Figs. 10 and 11.

In general, it is reported that the initial peak force increases consistently with indenter displacement, accompanied by a sequence of load drops associated with significant damages modes such as fiber failure and delamination. It can also be observed that the intensity of delamination signals observed in the baseline samples is higher than that of the filler-loaded samples which validates the correlation of damage area as seen in Fig. 9. In contrast, the filler-loaded samples exhibit delamination threshold load of 2550N, corresponding to 1.7mm indentation depth, while a sudden load drop was observed at 3280N, corresponding to 2.57mm. In practice, it was observed that the damage onset load and the fiber breakage load exhibited by the filler-loaded samples was for 19% and 15% higher than for the baseline samples. This result shows that damage initiation and accumulation were delayed for the filler-loaded sample comparing to the baseline samples. In Figs. 10 and 11, it can be observed that indentation depth of 3 mm results in compression fracture at the contact location of the indenter causes matrix shear cracking and fiber micro-buckling while delamination followed up by intra-laminar cracking and axial fiber splitting at the back side. In Fig. 9, it appears that the filler-loaded samples exhibit a reduced damage area than the baseline samples, and, moreover, the filler-loaded samples have higher contact stiffness and load carrying capacity than the baseline samples.

Figures 8 (a) to (f) show the load-displacement behavior of the baseline and the filler-loaded samples indented at 4, 5 and 6mm. The same trend was observed with a flat profile of the AE cumulative counts indicating the damage initiation stage and a steep rise in the slope of the curve showing the damage accumulation. It was observed that the damage onset load in the baseline samples occurred at an average of 2100 N at 1.2mm followed by a sudden load drop at 2700N and 1.8mm corresponding to the fiber failure. In contrast, the filler-loaded samples exhibited delamination damage load and a load drop related to fiber damage at 2500N and 1.6mm, and 3100N and 2.1mm, respectively. It is significant to observe that the damage onset load and the fiber breakage load exhibited by the filler-loaded samples were for about 20% and 15% higher than the baseline samples, respectively. This is due to enhanced energy dissipation through toughening mechanism such as filler/matrix debonding, filler interlocking/bridging which contributes to higher load-bearing capacity.

At a higher indentation depth, a fiber failure occurs during penetration/perforation of the samples which reduces the load resistance capability. Beyond 4 mm indentation depth, all the samples show the same trend in peak load and absorbed energy, while no significant increase was observed due to a more intense fiber failure. The failure occurred through matrix shear cracking, and fiber micro-buckling at the local contact of the indenter, followed by delamination between the adjacent plies and intra-laminar cracking (or) axial fiber splitting through penetration/perforation of the indenter. It is clearly seen that the

delamination onset load was almost similar for all the samples while the improvement in the fiber breakage load reduces drastically with an increasing indentation depth due to the perforation/penetration of the samples.
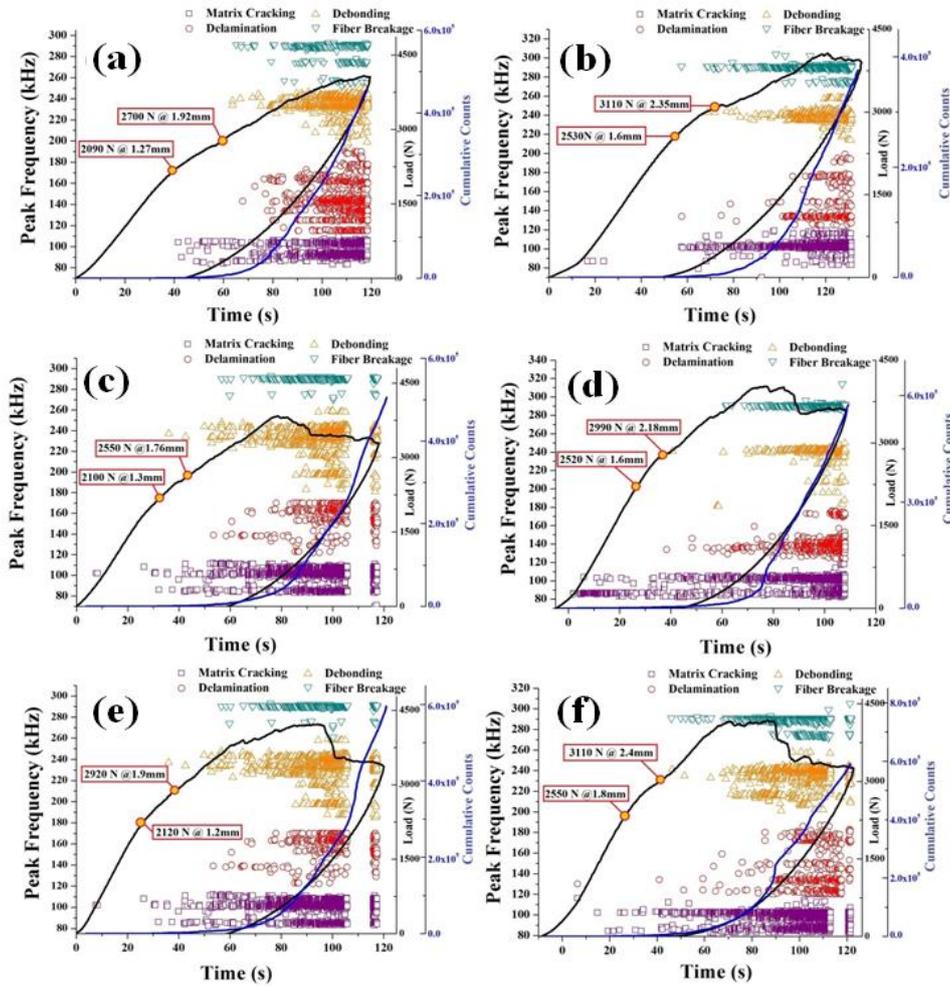
Fig. 8 Peak frequency & Cumulative Counts vs. Time plot of corresponding load-displacement behavior for indentation depth. Baseline samples: (a) 4mm (c) 5mm (e) 6mm & Filler-loaded Samples: (b) 4mm (d) 5mm (f) 6mm
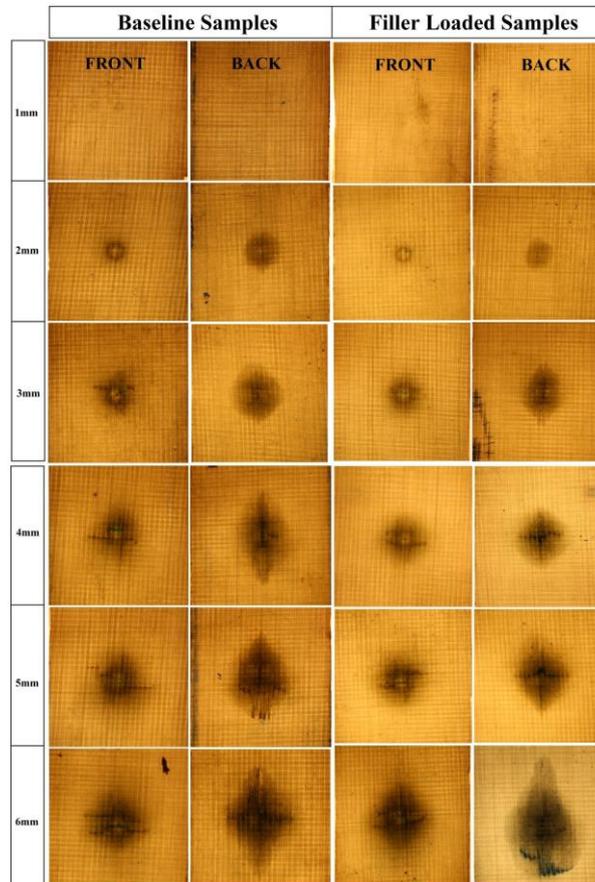
Fig. 9 Images of projected indentation damaged area at different indentation depth

Figures 10 and 11 show optical microscope images of the fractured surfaces observed during the quasi-static indentation test in the baseline and the filler-loaded samples. At a lower indentation depth, matrix fracture damage occurs, which decreases the localized stiffness of the laminate, but does not result in any catastrophic failure. However, further increasing the indentation displacement can cause the matrix cracking to progress into delamination and fiber breakage, due to the tensile stress caused by the indenter contact. In general, the transverse matrix cracking develops into delamination between the adjacent plies, and finally, prevalent intra-laminar crack and in-plane fiber buckling/breakage cause penetration and perforation damage at a higher indentation depth (4 to 6 mm). Figures 9, 10 and 11 show that the intensity of damage in the baseline samples was predominant comparing to the filler-loaded samples, especially at a higher indentation depth.

In contrast, the damage exhibited by the filler-loaded samples was minor and delayed, due to the improved load carrying capacity and energy absorption characteristics offered by the presence of fillers. Figures 12 (a) and (b) show scanning electron microscope images of the fractured surfaces of the baseline and the filler-loaded samples. The baseline samples

exhibit smooth and brittle fracture surface associated with no plastic deformation corresponding to low fracture toughness of epoxy matrix. However, the fracture surface of the filler-loaded samples indicates rough surface with intense scarps/river lines. The intense scarps/river lines indicate hindrance of crack growth. Figure 12 (b) shows the fillers strongly bonded to the matrix and filler debonding/pullout, which can be attributed to the additional energy dissipation mechanisms.
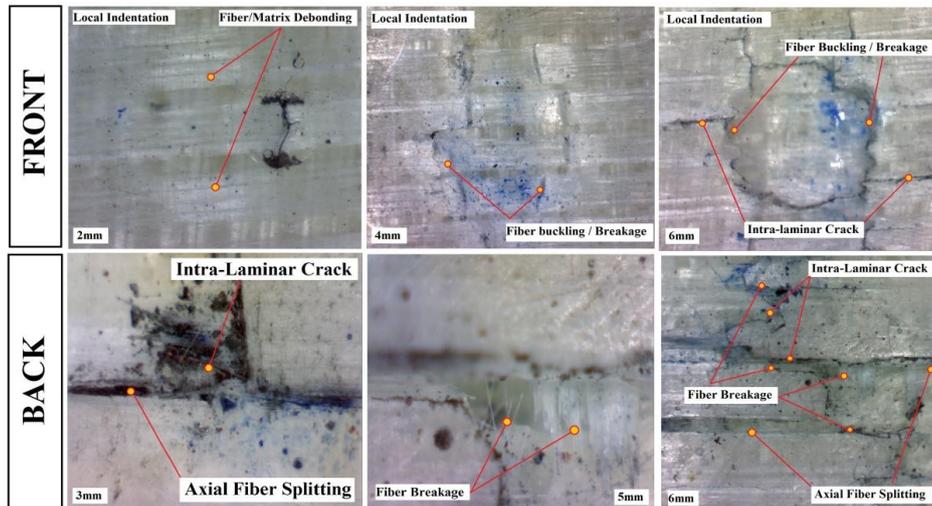
Fig. 10 Optical microscopic images of the fractured surfaces observed during quasi-static indentation test for baseline samples
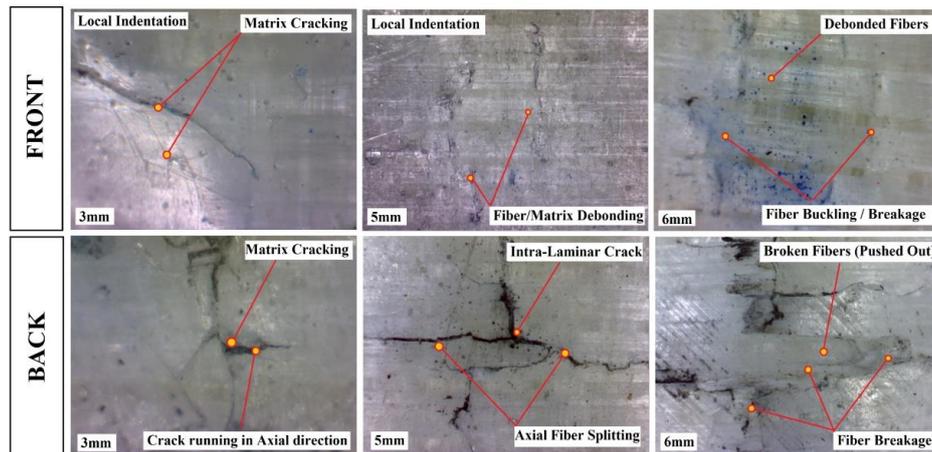
Fig. 11 Optical microscopic images of the fractured surfaces observed during quasi static indentation test for filler-loaded samples
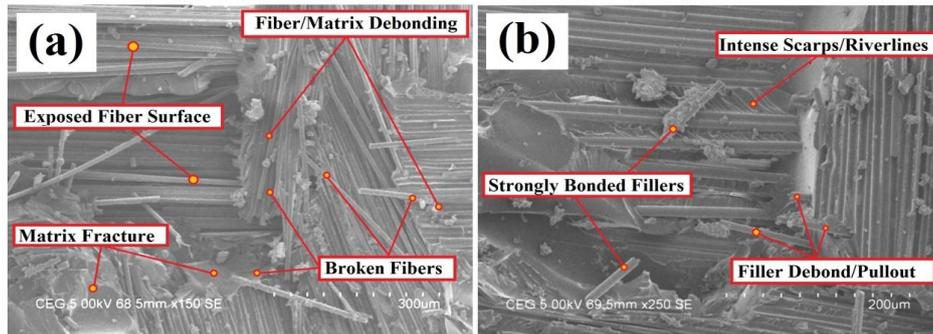
Fig. 12 SEM micrograph of the fractured surfaces showing: (a) Baseline samples (b) Filler-loaded samples

Online AE monitoring was also employed during the three-point bending test, to monitor the evolution of damage and to characterize the damage modes associated with flexural loading. Acoustic emission results of flexural after indentation and quasi-static indentation test showed mostly similar trends. Therefore, the results of the normalized number of AE Events for flexural after indentation test was illustrated to discuss the damage mechanisms.

Figure 13 shows the normalized number of AE events exhibited during flexural after indentation test associated with types of failure modes for baseline and filler-loaded samples. The damage mechanisms associated with flexural after indentation test were characterized from frequency ranges, as discussed above. It can be observed that the delamination signals intensity in the baseline samples are more intense and greater than the filler-loaded samples which validate the correlation between these data and those of the damage areas. It can be observed that the matrix cracking signals associated during the test were found to be concentrated and more intense since they start almost from the beginning of loading; this triggers the other failure modes in both the baseline and filler-loaded samples. The number of the AE events associated with the delamination signals for the baseline samples was found to be more intense comparing to the filler-loaded samples: this trend was observed to be prominent at a higher indentation depth (beyond 4 mm). It can be suggested that, at this point, quasi-static indentation on the glass/epoxy samples has caused sufficient delamination damage, which might progress during post-indentation flexural testing. Correspondingly, the number of the AE signals attributed to matrix cracking decreases, while those related to delamination increase for the samples indented beyond 4 mm. This evidences that during flexural loading, the damage initiates as matrix cracking in the non-indented samples and samples indented below 4 mm. In contrast, in the samples indented beyond 4 mm, the failure starts/develops from the former damage mode (usually delamination / debonding). Consequently, the debonding and fiber breakage signals observed in all other cases were almost similar, and no significant changes in the intensity of AE signals were observed as seen in Fig. 13(a).
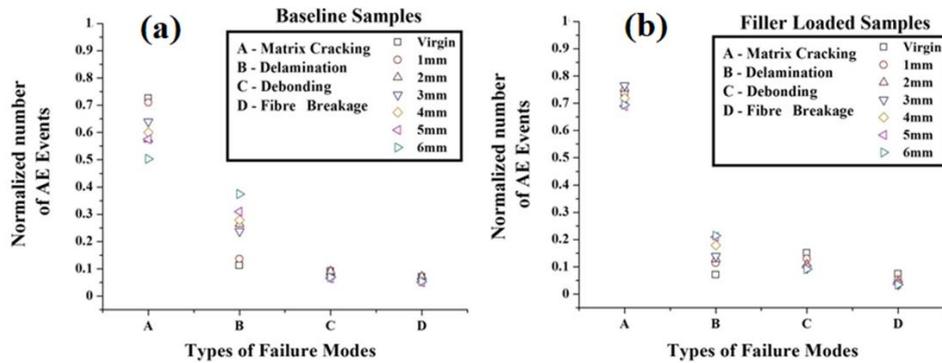
Fig. 13 Types of failure modes versus normalized number of AE events for Flexural After Indentation test: (a) Baseline Samples (b) Filler-loaded Samples

Similarly, Fig. 13 (b) shows the normalized number of the AE events with corresponding types of failure modes exhibited by the filler-loaded samples during flexural after indentation test. It can be observed that the normalized number of the AE events corresponding to the matrix cracking was highly predominant for the filler-loaded samples in all the cases (virgin and all indented samples). In contrast, the number of the AE events corresponding to delamination signals was observed to be lower for the filler-loaded samples than the baseline samples, even for the samples subjected to a higher indentation depth. However, the corresponding debonding signals associated with the test in the filler-loaded samples were greater than the baseline samples. This is due to the filler presence in the interlaminar domain introducing toughening mechanism, such as filler debonding/ pullout resulting in more intense debonding AE events. Subsequently, the number of the AE events related to the fiber breakage was almost similar in both the baseline and the filler-loaded samples for all the cases of flexural after indentation.

4. CONCLUSIONS

This present work investigates the influence of milled glass fiber filler on glass/epoxy samples subjected to quasi-static indentation and flexural after indentation tests with acoustic emission monitoring. The evolution of damage and characterization of damage mechanisms associated with loading were discussed, and the results were correlated with the baseline glass/epoxy samples.

The results show that, irrespective of indentation depth, the filler-loaded samples exhibited a slightly higher peak force for about an average of 10% than the baseline samples. In all the cases beyond 4 mm, no significant difference in the peak load was observed, corresponding to the predominant fiber damage during penetration/perforation of samples. The initial contact stiffness as well as the delaminated one of the filler-loaded samples was 2181 ± 75 N/mm and 955 ± 72 N/mm, respectively, while the baseline samples showed the initial and the delaminated contact stiffness of 1902 ± 58 N/mm and 832 ± 75 N/mm, respectively. The filler-loaded samples showed 15% improvement in the initial and the delaminated contact stiffness in comparison with the baseline samples.

It was observed that the filler-loaded samples exhibited a reduced permanent depth and a damage area by an average of 25% than the baseline samples. The presence of the filler offers greater rigidity/stiffness and higher energy absorption through plastic deformation and toughening mechanism, such as filler debonding/pullout, filler bridging/interlocking.

The residual flexural strength was observed to reduce gradually by an average of 15% for an indentation depth below 3 mm with a reduction of about 30% at a higher indentation depth in both the baseline and the filler-loaded samples, leading to a large delamination area and intensive fiber breakage causing penetration/perforation damage. This evidences that the beyond 3 mm, the load carrying capacity of the glass/epoxy samples decreases drastically due to the greater accumulated damage during indentation. Besides, the filler-loaded samples exhibited an average of 18% higher residual strength than the baseline samples.

Damage mechanisms associated with quasi-static indentation and flexural after indentation test, as characterized from AE frequency data, were almost similar. However, in the former the presence of delamination and debonding was more evident for the highest indentation depths than in the latter samples.

REFERENCES

1. Atas, C., Icten, B.M., Küçük, M., 2013, *Thickness effect on repeated impact response of woven fabric composite plates*, Compos Part B, 49, pp. 80–85.
2. Aktas, M., Atas, C., Icten, B.M., Karakuzu, R. 2009, *An experimental investigation of the impact response of composite laminates*, Compos Struct., 87(4), pp. 307–13.
3. Fragassa, C., 2017, *Marine Applications of Natural Fibre-Reinforced Composites: A Manufacturing Case Study*, In: Pellicer E, et al. (eds.), Advances in Application of Industrial Biomaterials, Springer, pp. 21-47.
4. Rohwer, K., 2016, *Models for intralaminar damage and failure of fiber composites - A review*, Facta Universitatis-Series Mechanical Engineering, 14(1), pp. 1-19.
5. Fragassa, C., Pavlovic, A., Vannucchi de Camargo, F., Minak, G., 2018, *Experimental evaluation of static and dynamic properties of low styrene emission vinylester laminates reinforced by natural fibres*, Polymer Testing, 69, pp. 437-449.
6. Fragassa, C., Pavlovic, A., Santulli, C., 2018, *Mechanical and impact characterisation of flax and basalt fibre bio-vinylester composites and their hybrids*, Composites - Part B, 137, pp. 247-259.
7. Flores Johnson, E.A., Li, Q.M., 2011, *Experimental study of the indentation of the sandwich panel with carbon fiber reinforced polymer face sheets and polymeric foam core*, Compos Part B, 42, pp. 1212-1219.
8. Xiao, J.R., Gama, B.A., Gillespie, J.W., 2007, *Progressive damage and delamination in plain weave S-2 glass /SC-15 composites under quasi-static punch-shear loading*, Compos Struct., 78, pp. 182-196.
9. Abdallah, A., Bouver, C., 2009, *Experimental analysis of damage creation and permanent indentation on highly oriented plates,* Compos Sci & Technol, 69, pp. 1238-1245.
10. Kaczmarek, H., Maison, S., 1994, *Comparative ultrasonic analysis of damage in CFRP under static indentation and low-velocity impact*, Compos Sci & Technol, 51, pp. 11-26.
11. Lee, S.M., Zahuta, P., 1991, *Instrumented impact and static Indentation of composites*, J. Compos Mater, 25, pp. 204-222.
12. He, W., Guan, Z., Li, X., Liu, D., 2013, *Prediction of permanent indentation due to impact on laminated composites based on an elastoplastic model incorporating fiber failure*, Compos Struct, 96, pp. 232-242.
13. Hachemane, B., Zitoune, R., Bezzazi, B., Bouvet, C., 2013, *Sandwich composites impact and indentation behavior study*, Compos Part B, 51, pp. 1-10.
14. Arabzadeh, H., Zeinoddini, M., 2013, *A closed-form solution for lateral indentation of pressurized pipes resting on a flexible bed*, International Journal of Mechanical Sciences, 75, pp. 189–199.
15. Sutherland, L.S., Guedes Soares, C., 2005, *Contact indentation of marine composites,* Composite Structures 70, pp. 287–294.
16. Potti, S.V., Sun, C.T., 1997, *Prediction of impact-induced penetration and delamination in thick composite laminates,* Int J Imp Eng, 19(1), pp. 31–48.

17. O'Masta, M.R., Crayton, D.H., Deshpande, V.S., Wadley, H.N.G., 2015, *Mechanisms of penetration in polyethylene reinforced cross-ply laminates,* International Journal of Impact Engineering, 86, pp. 249-264.

18. Suresh Kumar, C., Arumugam, V., Santulli, C., 2017, *Characterization of indentation damage resistance of hybrid composite laminates using acoustic emission monitoring*, Composites Part B, 111, pp. 165-178.

19. Singh, R.P., Zhang, M., Chan, D., 2002, *Toughening of a brittle thermosetting polymer, pp. effects of reinforcement particle size and volume fraction,* J Mater Sci, 37, pp. 781–8.

20. Wicks, S.S., de Villoria, R.G., Wardle, B.L., 2010, *Inter-laminar and intralaminar reinforcement of composite laminates with aligned carbon nanotubes*, Compos Sci Technol., 70, pp. 20–28.

21. Davis, D., Whelan, B., 2011, *An experimental study of inter-laminar shear fracture toughness of a nanotube-reinforced composite*, Compos Part B, 42, pp. 105–116.

22. Adams, R.D., Cawley, P., 1988, *A review of defect types and non-destructive testing techniques for composites and bonded joints,* NDT & E Inter, 21(4), pp. 201-222.

23. Fotouhi, M., Ahmadi, M., Oskouei, A.R., 2014, *Acoustic emission-based study to characterize the initiation of delamination in composite materials*, J Thermoplastic Compos Mater 2014, 1-9, DOI: 10.1177/0892705713519811.

24. Fotouhi, M., Pashmforoush, F., Ahmadi, M., 2011, *Monitoring the initiation and growth of delamination in composite materials using acoustic emission under quasi-static three- point bending test,* J Reinf Plast Compos., 30(17), pp. 1481-1493.

25. Grosse, C.U., Linzer, L.M., 2008, *Signal-based AE analysis, Acoustic Emission Testing*, Springer, pp. 53-99.

26. Bar, H.N., Bhat, M.R., Murthy, C.R.L., 2005, *Parametric analysis of acoustic emission signals for evaluating damage in composites using PVDF film sensors,* Journal of Nondestructive Evaluation, 24(4), pp. 121–134.

27. Bussiba, M., Kupiec, S., Ifergane, R., Piat, T., 2008, *Damage evolution and fracture events sequence in various composites by acoustic emission technique*, Compos. Sci. Technol. 68, pp. 1144–1155.

28. Ramirez-Jimenez, C.R., Papadakis, N., Reynolds, N., Gan, T.H., Purnell, P., Pharaoh, M., 2004, *Identification of failure modes in glass/polypropylene composites by means of the primary frequency content of the acoustic emission event*, Compos Sci Technol, 64, pp. 1819–27.

29. Asokan, R., Arumugam, V., Santulli, C., Barath Kumar, S., Stanley A.J., 2011, *Investigation of the strength of the failure modes in GFRP laminates using acoustic emission monitoring*, Int J Poly Technol, 3(2), pp. 57–65.

30. ASTM D 6264/D6264 M-2017, Test method for measuring the damage resistance of a fiber-reinforced polymer-matrix composite to a concentrated quasi-static indentation force.

31. Arumugam, V., Sajith, S., Stanley, A.J., 2011, *Acoustic Emission Characterization of Failure Modes in GFRP Laminates Under Mode I Delamination*, J Nondestructive Eval, 30(3), pp 213–219.

32. Hafeez, F., Almaskari, F., 2015, *Experimental investigation of the scaling laws in laterally indented filament wound tubes supported with V-shaped cradles*, Composite Structures, 126, pp. 265–284.

33. Gama, B.A., Islam, S.M.W., Rahman, M., Gillespie, J.W., et al., 2005, *Punch shear behavior of thick-section composites under quasi-static, low velocity, and ballistic impact loading*. SAMPE J, 41(4), pp. 6–13.

34. Jefferson, A.J, Arumugam, V., Saravanakumar, K., Dhakal, H.N., Santulli, C., 2015, *Compression after impact strength of repaired GFRP composite laminates under repeated impact loading*, Compos Struct, 133, pp. 911–20.

35. Mitrevski, T., Marshall, I.H., Thomson, R., Jones, R., Whittingham, B., 2005, *The effect of impactor shape on the impact response of composite laminates*. Compos Struct, 67, pp. 139-148.

36. Zhang, Z.Y., Richardson, M.O.W., 2007, *Low velocity impact induced damage evaluation and its effect on the residual flexural properties of pultruded GRP composites*, Compos Struct, 81, pp. 195-201.

37. Heidary H., Ahmadi M., Rahimi A, Minak G,, 2013, *Wavelet-based acoustic emission characterization of residual strength of drilled composite materials*, J Compos Mater 47, pp. 2897-2908.

38. Petrucci, R., Santulli, C., Puglia, D., Nisini, E., Sarasini, F., Tirillò, J., Torre, L., Minak, G., Kenny, J.M., 2015, *Impact and post-impact damage characterisation of hybrid composite laminates based on basalt fibres in combination with flax, hemp and glass fibres manufactured by vacuum infusion*, Compos Part B, 69, pp. 507-515.

39. Mohammadi, R., Najafabadi, M.A., Saeedifar, M., Yousefi, J., Minak, G., 2017, *Correlation of acoustic emission with finite element predicted damages in open-hole tensile laminated composites*, Compos Part B, 108, pp. 427-435.